Original Article

JCBFM

Journal of Cerebral Blood Flow & Metabolism
2022, Vol. 42(2) 338–348

DOI: 10.1177/0271678X21048031
journals.sagepub.com/home/jcbfm
SAGE

Brain oxygen extraction fraction mapping in patients with multiple sclerosis

Junghun Cho[1], Thanh D Nguyen[1], Weiyuan Huang[1], Elizabeth M Sweeney[2], Xianfu Luo[1], Ilhami Kovanlikaya[1], Shun Zhang[1], Kelly M Gillen[1], Pascal Spincemaille[1], Ajay Gupta[1], Susan A Gauthier[1,3] and Yi Wang[1,4]

Abstract

We aimed to demonstrate the feasibility of whole brain oxygen extraction fraction (OEF) mapping for measuring lesion specific and regional OEF abnormalities in multiple sclerosis (MS) patients. In 22 MS patients and 11 healthy controls (HC), OEF and neural tissue susceptibility (χ_n) maps were computed from MRI multi-echo gradient echo data. In MS patients, 80 chronic active lesions with hyperintense rim on quantitative susceptibility mapping were identified, and the mean OEF and χ_n within the rim and core were compared using linear mixed-effect model analysis. The rim showed higher OEF and χ_n than the core: relative to their adjacent normal appearing white matter, OEF contrast $= -6.6 \pm 7.0\%$ vs. $-9.8 \pm 7.8\%$ ($p < 0.001$) and χ_n contrast $= 33.9 \pm 20.3$ ppb vs. 25.7 ± 20.5 ppb ($p = 0.017$). Between MS and HC, OEF and χ_n were compared using a linear regression model in subject-based regions of interest. In the whole brain, compared to HC, MS had lower OEF, $30.4 \pm 3.3\%$ vs. $21.4 \pm 4.4\%$ ($p < 0.001$), and higher χ_n, -23.7 ± 7.0 ppb vs. -11.3 ± 7.7 ppb ($p = 0.018$). Our feasibility study suggests that OEF may serve as a useful quantitative marker of tissue oxygen utilization in MS.

Keywords

Oxygen extraction fraction, multiple sclerosis, quantitative susceptibility mapping, quantitative blood oxygenation level dependent magnitude, QSM+qBOLD

Received 22 April 2021; Revised 3 August 2021; Accepted 30 August 2021

Introduction

Multiple sclerosis (MS) is an inflammatory demyelinating disease of the white matter (WM) with progressive neurodegeneration and is a leading cause of neurological disability in young adults.[1] MRI has been the standard in vivo imaging technique for diagnosing MS and monitoring disease progression.[2,3] New acute MS lesions develop near the disrupted brain blood barrier (BBB) and appear hyperintense on Gadolinium-enhanced T1-weighted image (T1w+Gd)[3,4] as a consequence of contrast agent leakage. Following BBB repair, lesions are characterized by a non-enhancing status on T1w+Gd; these lesions are typically regarded as chronic and appear hyperintense on T2-weighted fluid-attenuated inversion recovery (T2FLAIR) image. This is attributable to demyelination and axonal loss.[2,3]

Recently, an important subset of chronic MS lesions has been identified which exhibit low-grade sustained microglial activity and expanding demyelination at the lesion rim.[5–7] These so-called chronic active lesions have been associated with increased tissue damage, neuroinflammation, and disability,[8] and may be a

[1]Department of Radiology, Weill Cornell Medicine, New York, NY, USA
[2]Department of Population Health Sciences, Weill Cornell Medicine, New York, NY, USA
[3]Department of Neurology, Weill Cornell Medicine, New York, NY, USA
[4]Department of Biomedical Engineering, Cornell University, Ithaca, NY, USA

Corresponding author:
Yi Wang, 407 East 61st St, Suite 118, New York, NY 10065, USA.
Email: yiwang@med.cornell.edu

driving factor in progressive disease.[9,10] Quantitative susceptibility mapping (QSM)[11] has been used to detect these lesions based on their characteristic paramagnetic rim appearance (QSM rim+) owing to its sensitivity to the iron-rich pro-inflammatory microglia and macrophages in the rim region.[9,12–18] However, the metabolic activity of these immune cells has yet to be measured with current imaging techniques such as PET (due to limited spatial resolution) and conventional MRI (due to lack of sensitivity).

The primary objective of this study was to demonstrate the feasibility of whole brain mapping of oxygen extraction fraction (OEF) in MS patients using a widely available multi-echo gradient echo (mGRE) sequence and a novel integrated model of QSM phase signal and quantitative blood oxygenation level dependent magnitude signal (qBOLD) (QSM+qBOLD, or QQ).[19,20] QQ separates the effect of deoxyheme iron in a cylindrical micron-scale venule (OEF effect) from that of neural tissue susceptibility (χ_n) contributed for example by the diffuse nano-scale ferritin iron in tissue, based upon their unique contributions to tissue susceptibility determined on QSM[21–23] and to the magnitude signal decay as modeled by qBOLD.[24–27] QQ has been shown to provide OEF measurements that are in good agreement with dual-gas calibrated BOLD[28] and the gold standard ^{15}O PET-OEF.[29]

In our study, we aim to demonstrate the potential of QQ to provide a quantitative marker of oxygen metabolism in the rim area of QSM rim+ lesions, which may be useful in the development of new therapeutic targets to reduce inflammation in chronic active lesions. As a secondary objective, QQ-based OEF mapping is used to investigate regional oxygen metabolism differences in cortical gray matter (CGM) and deep gray matter (DGM) between MS patients and healthy controls (HCs), which have been implicated in neurodegenerative processes and are regarded as major indicators of tissue injury and neuronal loss in MS.[30–36]

Materials and methods

Study cohort

This retrospective image analysis study was approved by the Weill Cornell Medicine local Institutional Review Board, and written informed consent was obtained from all individuals in accordance with the ethical standards of the Helsinki Declaration of 1975 and its later amendments. MS patients were selected from an ongoing imaging and clinical MS research database and were diagnosed according to the McDonald criteria.[3] A total of 22 relapsing-remitting MS patients with at least one chronic active QSM rim+ lesion was included (17 females, 5 males; mean age, 37 ± 6 years). In addition, 11 age-matched HCs (1 female, 10 males; mean age, 34 ± 12 years) were included for comparison. The demographic and clinical characteristics of the study participants, e.g. expanded disability status scale (EDSS) to evaluate the functional systems of the central nervous system (0 = normal neurologic status, 10 = death due to MS),[37] are summarized in Table 1.

Table 1. Clinical and demographic characteristics of the study cohort. Age, disease duration, and expanded disability status scale (EDSS) score are shown as mean ± standard deviation (minimum-maximum).

Variable	Healthy controls	MS patients	P-value
Number	11	22	
Number of women[a]	1 (9%)	17 (77%)	<0.001[a]
Age (years)[b]	34 ± 12 (22–63)	37 ± 6 (28–52)	0.19[b]
Disease duration (years)	N.A.	16 ± 12 (1–40)	
EDSS score	N.A.	1.4 ± 1.1 (0–3.5)	
MS phenotype	N.A.	Relapsing-remitting	
Medical treatment[c]	N.A.	21 (95%)	

[a]χ^2 test.
[b]Wilcoxon rank sum test.
[c]Medical treatment includes Gilenya (N = 3), Ocrevus (N = 9), Tecfidera (N = 3), Tysabri (N = 4), and Copaxone (N = 2).

MRI protocol

All brain MRIs were performed on a 3 T GE scanner. The typical MS imaging protocol consisted of 3 D sagittal T1w and T1w+Gd (field of view (FOV) = 24 cm, TR = 8.8 ms, TE = 3.4 ms, TI = 450 ms, flip angle (FA) = 15°, voxel size = $1.2 \times 1.2 \times 1.2\,mm^3$), 2 D axial T2w (FOV = 28 cm, TR = 5917 ms, TE = 88 ms, flip FA = 90°, voxel size = $0.7 \times 1.2 \times 3\,mm^3$), and 3 D T2FLAIR (FOV = 24 cm, TR = 6050 ms, TE = 149.4 ms, TI = 1820 ms, FA = 90°, voxel size = $1.2 \times 1.2 \times 1.2\,mm^3$) for anatomy and lesion detection, as well as 3 D mGRE for QSM and OEF mapping (FOV = 24 cm, TR = 57.5 ms, TE1/ΔTE = 4.5/4.8 ms, number of TEs = 11, FA = 20°, voxel size = $0.7 \times 0.9 \times 3\,mm^3$, axial slice acquisition parallel to B0 direction).

The imaging protocol for HCs consisted of axial 3 D mGRE (FOV = 20 cm, TR = 30.5 ms, TE1/ΔTE = 2.3/3.9 ms, number of TEs = 7, FA = 15°, voxel size = $1.2 \times 1.2 \times 1.2\,mm^3$, flow-compensated in all three directions,[38] axial slice acquisition parallel to B0 direction) and 3 D T1w (FOV = 20 cm, TR = 7.7 ms, TE = 2.9 ms, TI = 450 ms, FA = 15°, voxel size = $0.8 \times 0.8 \times 1.2\,mm^3$).

Image processing and analysis

QSM reconstruction consisted of total field estimation from the mGRE phase data by linear fitting,[39]

background field removal using Projection onto Dipole Fields (PDF) algorithm,[40] and inversion of the local field to obtain the susceptibility distribution using Morphology Enabled Dipole Inversion with automatic uniform cerebrospinal fluid zero reference (MEDI + 0) algorithm.[11,41–43] In HCs, the total field was estimated using an adaptive quadratic-fit of the mGRE phase to benefit from 3 D flow-compensation.[38]

OEF and neural tissue susceptibility (χ_n) maps were computed from QSM and mGRE magnitude data using the QQ algorithm.[19,20] QQ unifies two biophysical models of mGRE data:[19] 1) a QSM-based model which distinguishes the susceptibility contribution of blood (determined by its oxygenation level) from that of neural tissue [22,23,44] on a per voxel basis, and 2) qBOLD which models the mGRE magnitude signal decay by the field variation inside a voxel based on the susceptibility difference between blood and the surrounding tissue.[24–27,45–47]

To improve the robustness of QQ against noise in the data fitting, the original cluster analysis of time evolution (CAT) algorithm[20] was refined by incorporating a brain/CSF segmentation into clustering.[48,49] This segmentation was obtained from the echo-combined magnitude mGRE image using the FSL FAST segmentation algorithm.[50] The CAT method groups voxels of the same tissue type with similar temporal mGRE magnitude evolutions into a cluster that are assumed to have similar model parameter values including OEF. Then, cluster-wise optimization is performed to solve for the model parameters. Total variation denoising[51] was applied to enhance the effective signal-to-noise ratio of OEF reconstruction.

For MS lesion-specific OEF analysis, two neuroradiologists (S.Z., 6 years of experience and W.H., 11 years of experience) identified lesions on T2FLAIR and manually traced QSM rim+ lesions on QSM based on their relative contrast with respect to the adjacent normal appearing white matter (NAWM).[12,13] To exclude both regional variation within a subject and inter-subject variation, the average OEF within each lesion was referenced to the average of its adjacent NAWM, OEF contrast (OEFC) $= \overline{OEF} - \overline{OEF_{NAWM}}$. Lesion χ_n contrast was defined in the same way ($\chi_n C = \overline{\chi_n} - \overline{\chi_{n,NAWM}}$). The average and standard deviation of $\overline{\chi_{n,NAWM}}$ among all the lesions was -21.9 ± 13.8 ppb. For each QSM rim+ lesion, the central veins were removed, and the hyperintense rim area in QSM was traced as lesion rim by three neuroradiologists (S.Z., 6 years of experience, W.H., 11 years of experience, and I.K., 23 years of experience), with the

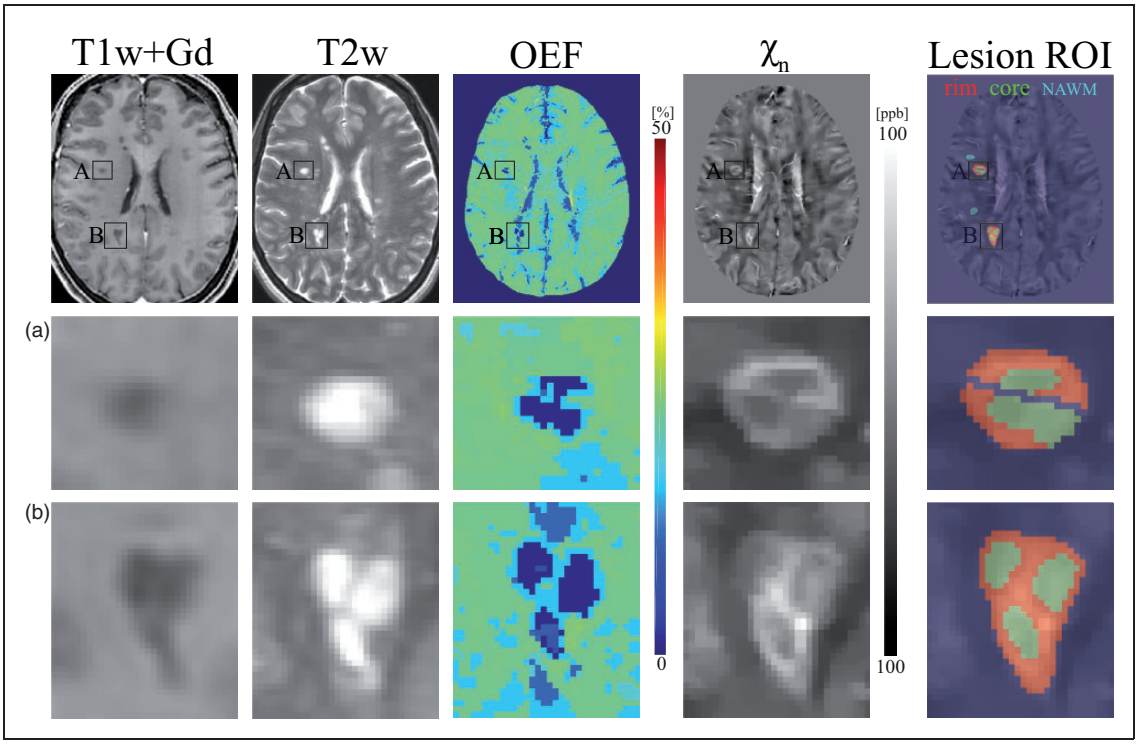

Figure 1. Example of T1w+Gd image, T2w image, OEF and neural tissue susceptibility (χ_n) maps obtained from an MS patient (disease duration, 11 years) showing two chronic active lesions with paramagnetic rims (A and B). In both lesions, the rim regions (red) show higher OEF and χ_n than the core regions (green). The central vein within lesion A is excluded from the lesion ROI. Normal appearing white matter (NAWM) mask for each lesion is shown in cyan blue in lesion ROI map.

remaining part of the lesion defined as the lesion core. No significant blooming artifact were found near the lesions in the susceptibility maps (Figures 1 and 3). The blooming artifact seen on the gradient echo magnitude images is caused by the field inhomogeneity in the vicinity of a strong susceptibility source such as iron or air-tissue interface. The field can be described mathematically as the spatial convolution of the susceptibility source with a dipole kernel. QSM deconvolves the field to remove the blooming artifact and reveal the true susceptibility.[52] Acute T1w+Gd enhancing lesions were excluded from analysis. To compare OEF between HC and MS patients, FreeSurfer analysis of T1w anatomical images was used to obtain regions of interest (ROIs)[53] including cortical gray matter (CGM) and selective DGM including thalamus, caudate, putamen, and pallidum, which have been shown to be associated with neuronal loss and atrophy in MS.[30–33,35,54] MS lesions were excluded from these ROIs.

Statistical analysis

For QSM rim+ lesions, a linear mixed-effect model with a random effect for patient was used to assess the OEFC between the rim and core regions (core = 0, rim =1), adjusting for lesion volume. The random effect for patient accounts for the correlation within a patient. For OEF comparison between HC and MS, linear regression models were fit for each ROI (whole brain, CGM, and DGM), with average OEF in the region as the dependent variable and an indicator of MS versus HC (0 = HC, 1 = MS), gender (female = 0, male = 1), and age as independent variables. Multiple comparisons correction was performed using the false discovery rate.[55] The Jarque-Bera test confirmed the normality of each ROI data distribution (all p-values > 0.09).[56] A p-value of less than 0.05 was considered statistically significant. The same analyses were performed for χ_n.

Results

In MS patients, a total of 80 chronic QSM rim+ lesions were identified. Of these, the mean lesion volume was $440.0 \pm 431.0\,mm^3$, and the mean volume of rim and core regions was $267.0 \pm 267.4\,mm^3$ and $172.9 \pm 185.4\,mm^3$, respectively.

Figure 1 shows a representative case with two QSM rim+ lesions, showing higher OEF and χ_n in the rim region compared to the core region. Over 80 QSM rim+ lesions, the mean OEF and χ_n in the rim region was found to be significantly higher than that in the core region in the linear mixed-effect model analyses (Figure 2): OEFC = $-6.6 \pm 7.0\%$ vs. $-9.8 \pm 7.8\%$

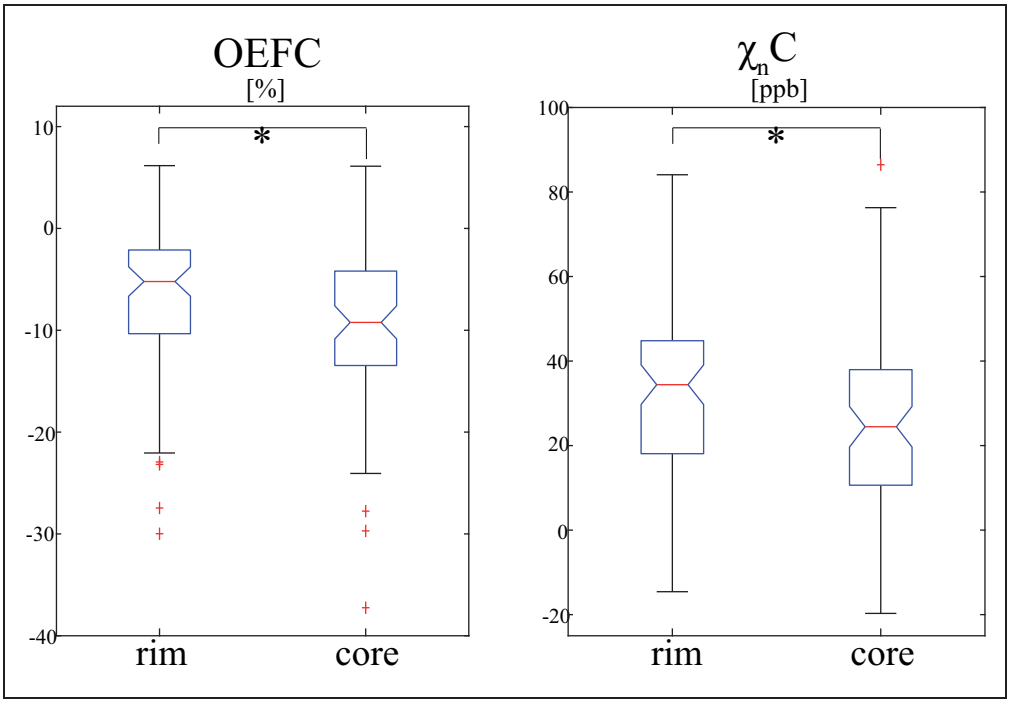

Figure 2. Comparison of mean OEF and neural tissue susceptibility (χ_n) contrast relative to adjacent normal appearing white matter (OEFC and χ_nC) between the rim and core regions of QSM rim+ lesions (n = 80). The rim region showed significantly higher mean OEFC and χ_nC than the core region in linear mixed-effect model analysis. Red line, blue box, black whisker, and red cross indicates median value, interquartile range, the range extending to 1.5 of the interquartile range, and outlier beyond the whisker range. Asterisk (*) indicates the significant difference ($p < 0.05$, linear mixed-effect model).

($\beta = 0.037$, 95% CI: [0.023, 0.051], $p < 0.001$) and $\chi_n C = 33.9 \pm 20.3$ ppb vs. 25.7 ± 20.5 ppb ($\beta = 0.007$, 95% CI: [0.001, 0.013], $p = 0.017$). Between MS and HC, the clusters appear similar, consisting mainly of GM, NAWM, and WM lesions (in MS subjects) (Supporting Information Figure S1). MS lesions with rim appearance tend to have distinctive clusters corresponding to the rim and core regions.

The lesion volume remained a significant covariate for OEFC ($\beta = -0.011$, 95% CI: [−0.019, −0.003], $p = 0.009$), but not for $\chi_n C$ ($p = 0.172$). The χ_n map was very similar to the QSM map (not shown) with an approximately 5 ppb difference (Figures 1 and 3).

Both HCs and MS patients generally show uniform OEF maps except for lesions and GM/WM contrast in χ_n maps (Figure 3). Compared to HCs, MS patients had significantly lower OEF values (Figure 4) as revealed by the linear regression model analyses: $30.4\% \pm 3.3\%$ vs. $21.4 \pm 4.4\%$ ($\beta = -0.099$, 95% CI: [−0.143, −0.055], $p < 0.001$) in whole brain, $29.9 \pm 2.9\%$ vs. $19.9 \pm 4.3\%$ ($\beta = -0.112$, 95% CI: [−0.153, −0.071], $p < 0.001$) in CGM, $31.3 \pm 3.5\%$ vs. $23.3 \pm 4.3\%$ ($\beta = -0.086$, 95% CI: [−0.130, −0.042], $p = 0.001$) in thalamus, $31.7 \pm 3.0\%$ vs. $23.3 \pm 3.6\%$ ($\beta = -0.088$, 95% CI: [−0.125, −0.051], $p < 0.001$) in caudate, $31.5 \pm 3.2\%$ vs. $24.6 \pm 3.9\%$ ($\beta = -0.072$, 95% CI: [−0.111, −0.033], $p = 0.002$) in putamen, $31.0 \pm 3.5\%$ vs. $25.2 \pm 3.4\%$ ($\beta = -0.052$, 95% CI: [−0.089, −0.015], $p = 0.012$) in pallidum. Gender and age were not significant covariates: p-values ≥ 0.751 for gender and ≥ 0.738 for age.

MS patients showed significantly higher χ_n values in the whole brain, -23.7 ± 7.0 ppb vs. -11.3 ± 7.7 ppb ($\beta = 0.010$, 95% CI: [0.002, 0.018], $p = 0.018$) and CGM, -23.3 ± 7.4 ppb vs. -7.1 ± 8.0 ppb ($\beta = 0.015$, 95% CI: [0.007, 0.023], $p = 0.003$) than HCs (Figure 4), whereas χ_n values were comparable in DGM: -12.6 ± 10.4 ppb vs. -12.9 ± 10.6 ppb ($p = 0.599$) in thalamus, 38.7 ± 10.2 ppb vs. 42.2 ± 14.0 ppb ($p = 0.613$) in caudate, 21.5 ± 13.5 ppb vs. 15.8 ± 16.6 ppb ($p = 0.055$) in putamen, and 86.9 ± 19.9 ppb vs. 84.8 ± 22.8 ppb ($p = 0.201$) in pallidum. Gender and age were not significant covariates: p-values ≥ 0.583 for gender and ≥ 0.494 for age.

Discussion

Our feasibility study demonstrated that high-resolution OEF maps can be extracted from mGRE data using the QQ algorithm for the study of global and regional tissue oxygen utilization in MS brains. We showed for the first time an OEF increase in the rim region compared to the core region in chronic active MS lesions with paramagnetic rim appearance. As QSM has become a reliable imaging tool for measuring

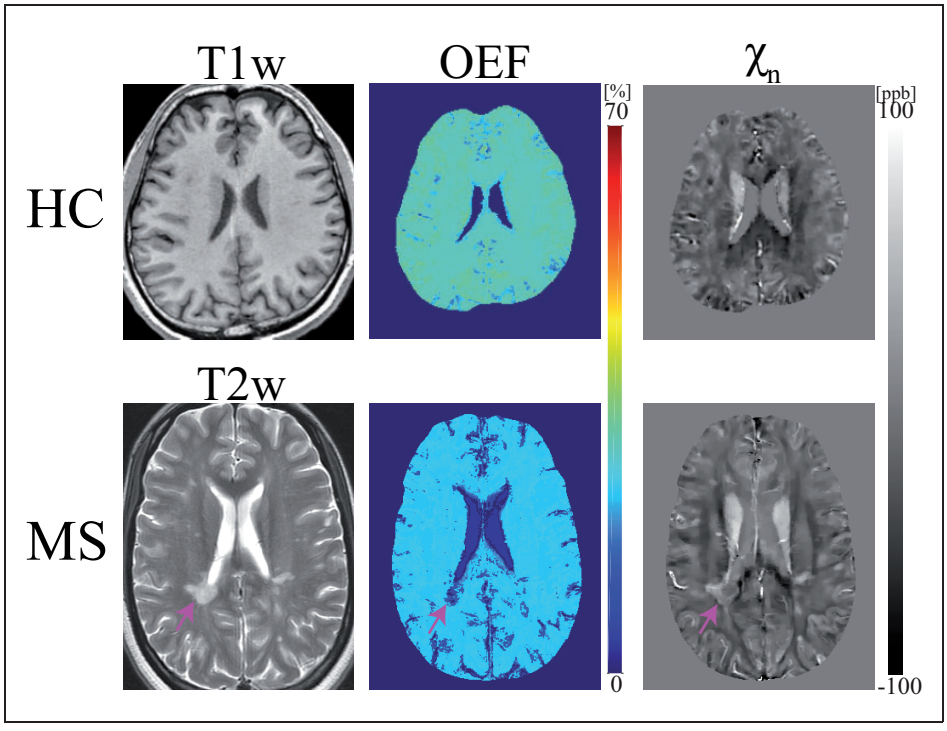

Figure 3. Exemplary OEF and neural tissue susceptibility (χ_n) maps obtained in HC and an MS patient (disease duration, 2 years). Pink arrow indicates a QSM rim+ lesion with a hyperintense rim consistent with iron-rich activated microglia. Brain OEF map for both subjects appears uniform except in lesion areas.

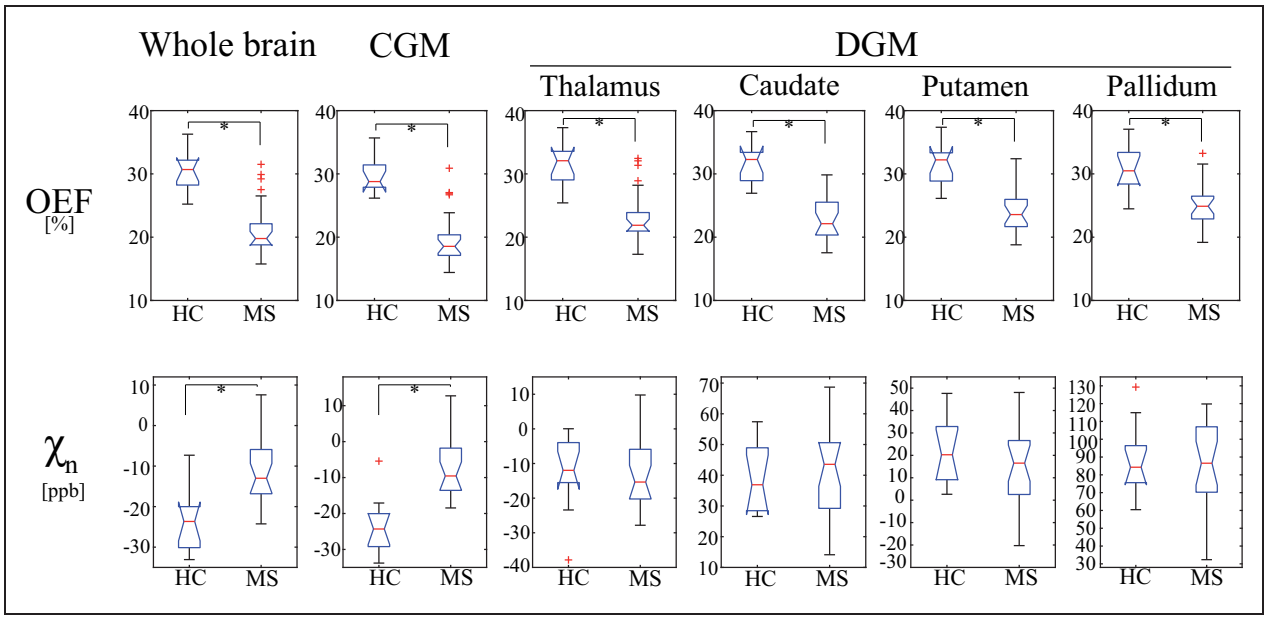

Figure 4. Comparison of average OEF and neural tissue susceptibility (χ_n) in whole brain, cortical gray matter (CGM), and select deep gray matter (DGM, thalamus, caudate, putamen, pallidum) between healthy controls (HC, 34 ± 12 years, n = 11) and MS patients (37 ± 6 years, n = 22). Asterisk (*) indicates significant difference ($p < 0.05$, linear regression model). Red line, blue box, black whisker, and red cross indicates median value, interquartile range, the range extending to 1.5 of the interquartile range, and outlier beyond the whisker range, respectively.

susceptibility changes in the brain, the ability to further separate the contributions of blood deoxyheme iron and neural tissue to tissue susceptibility by the QQ algorithm has the potential to provide a more comprehensive picture of both tissue oxygenation status and change in tissue iron and/or myelin content in chronic active MS lesion.[9,12–17]

In QSM rim+ lesions, the rim region was found to have significantly higher mean OEF and χ_n values than the core region (Figures 1 and 2). This difference is consistent with the histological evidence of higher density of iron-rich microglial cells in the lesion rim and PET imaging findings showing increased overall inflammatory activity in chronic active rim lesions.[8,12,16,57] The lower OEF observed in the core area of these lesions is also consistent with the irreversible tissue damage seen on histopathology.[8,10,57] These promising results suggest that OEF derived from mGRE data may serve as a sensitive marker of tissue oxygen metabolism in QSM rim+ lesions, which can be important for lesion status monitoring and development of novel MS therapeutic targets.

In both HCs and MS patients, brain OEF maps generally appear uniform except in lesions (Figure 3). This observation is consistent with OEF maps that were obtained by the reference standard ^{15}O PET,[58,59] which supports the presence of an equilibrium between metabolic needs and blood flow in the resting state.[59]

The observed lower global OEF obtained by the QQ algorithm in MS brains as compared to HCs (Figures 3 and 4) agrees well with the previously reported reduced OEF in MRI,[34,35,60] near-infrared spectroscopy,[60] and PET studies.[61] Lower OEF may represent a unique tissue injury mechanism underlying progressive demyelination and neurodegeneration in the MS brain. Several studies have indicated that impaired mitochondrial function via nitric oxide overproduction likely induces chronic oxygen deprivation in neuronal cells, which may result in neuronal dysfunction.[62–65]

Compared to a previous MRI-based OEF study using vein susceptibility modeling,[35] cortical OEF values in our study were similar for HCs, 29.9 ± 2.9 vs. 31.5 ± 3.0%, but lower for MS patients, 19.9 ± 4.3 vs. 28.1 ± 3.0%, which may be explained by the longer disease duration of our cohort (16 vs. 8.5 years).[35] Significantly lower OEF in frontal, temporal, parietal, and occipital CGM in MS, compared to HC (Supporting Information Figure S2), agrees with lower OEF observed in regional cortices, e.g. sensorimotor, parietal, and prefrontal cortex, with using the vein susceptibility modeling.[35] Furthermore, our global OEF was lower for both HCs (30.4 ± 3.3 vs. 38.6 ± 4.1%) and patients (21.1 ± 4.4 vs. 32.8 ± 5.2%) compared to a study using venous T2 modeling.[34] This discrepancy may be explained by the complexity in estimating oxygenation from T2 modeling. For

instance, performance of T2 oxygenation modeling is strongly dependent on accurate calibration of its model parameters.[66]

In DGM, MS patients have lower OEF values than HCs (Figure 4), which may be associated with tissue loss in those regions in MS brains.[30,32,67] For instance, the lower OEF in the thalamus, a central link for cortical-subcortical circuits,[68] may be related to thalamic neuronal loss[33] and atrophy,[69] which are predictors of long-term disability progression in MS.[70]

QSM sensitivity to tissue iron[71–73] has been applied to study MS brain tissue.[57,74] The susceptibility values of several deep gray nuclei (e.g. caudate and globus pallidus) in MS brains have been reported to be higher compared to HC.[67,74] This study furthers our understanding of QSM as it separates QSM into the contribution of oxygen metabolism (OEF effect) and neural tissue (χ_n effect). While OEF is reduced in all deep gray nuclei of MS brains, χ_n is not significantly changed compared to HC, unlike previous literature.[67,74] This may be due to the longer disease duration of subjects in this study, as iron content of deep gray nuclei in MS brains decreases as disease duration increases, while iron content in HC brains increases or remains stable.[73,75] Additional studies may be needed as there is no agreement in the literature on QSM values in the thalamus and putamen in MS as compared to HC.[67,74]

Both HC and MS showed generally higher χ_n in CGM compared to WM (Figure 3). This contrast is in line with the lower myelin and higher iron content in CGM.[76] However, compared to HC, χ_n was significantly higher in the whole brain and CGM of the MS brains, whereas OEF was lower (Figure 4). The biological cause of higher χ_n in CGM remains to be elucidated, though it may be related to iron accumulation and/or demyelination.[57,77]

This study has several limitations. First, the patient cohort is small and limited to relapsing-remitting MS with low EDSS. For instance, OEF was not significantly correlated with disease duration in all the ROIs (uncorrected p-values > 0.538, Spearman correlation analysis) (Supporting Information Figure S3) unlike a previously reported negative correlation.[35] This may be caused by a small number of patient cohort. Also, no significant correlation was found between OEF and EDSS in this study (Supporting Information Figure S3), whereas cortical OEF negatively correlated with EDSS in the previous venous OEF study.[35] This may be caused by a limited and low range of EDSS in this study (0-4).

Second, HC subjects had a different gender ratio from MS subjects which may affect the comparison result between HC and MS. To address the lack of female subjects in the HC group, we performed additional analysis to compare OEF only in the male subjects between HC ($n = 10$) and MS ($n = 5$) groups adjusting for age. We found that the MS group still showed significantly lower whole brain OEF than the HC group: $30.9\% \pm 3.2\%$ vs. $18.7 \pm 1.3\%$ ($\beta = -0.119$, 95% CI: $[-0.153, -0.085]$, $p < 0.001$). Furthermore, while females generally have lower hemoglobin concentration [Hb] and higher CBF than males,[78] prior literature in healthy adults shows that OEF in women is slightly higher[79] or similar[80] compared to OEF in men. These data suggest that the lower OEF observed in the MS group with more female subjects compared to the HC group is not driven by gender. Unfortunately, we could not obtain [Hb] or CBF measurements in our study.

Third, QQ has some modeling assumptions: the random cylinder orientation of the venous microvasculature in qBOLD of QQ may not be valid in MS lesions and therefore induce bias in OEF estimations. Although intracranial and extracranial vascular abnormalities have not been found in MS compared to HC,[81–83] microvascular abnormalities should be further investigated and potentially incorporated into QQ. Also, QQ does not consider detailed microstructure of the brain tissue including myelin, which may lead to a bias in OEF estimation. This may be a confounding factor in the comparison between MS and HC due to the demyelination and axonal loss in MS. QQ assumes two source compartments in a voxel, deoxyhemoglobin in venous structure and medium, such as diffusively distributed non-blood tissue ferratin or protein. If other structured strong sources including myelin in WM exists, additional introvoxel field variation would be induced, which may lead to greater MRI signal decay than the sole deoxyhemoglobin effect of venous blood. Consequently, QQ-based OEF may be overestimated in WM. However, in a validation study of QQ against the reference standard ^{15}O-PET, the OEF difference between QQ and PET was not significant in WM.[29] This may suggest that the myelin effect in QQ-based OEF estimation may not be significant.

Fourth, vein voxels (blood only) were treated the same way as brain voxels (mixture of neural tissue and blood), which could influence the accuracy of OEF and χ_n estimations in large veins. This could be mitigated by segmenting large veins; additional studies are needed to perform accurate vein segmentation.

Fifth, different scan protocols between HC and MS patients, e.g. longer TE range, no flow compensation, and lower slice resolution in MS, may affect the OEF comparison between HC and MS patients. Additional OEF processing was performed to investigate the effects of scan parameters on OEF comparison. When MS data were processed using a similar TE range ($TE_1/\Delta TE/TE_6 = 4.7/4.8/28.5$ ms) compared to

that of HC ($TE_1/\Delta TE/TE_7 = 2.3/3.9/25.7$ ms), we found lower OEF values in MS than HC, e.g. $23.0 \pm 3.2\%$ vs. $30.4 \pm 3.5\%$ for whole brain average OEF, in good agreement with the original findings (Supporting Information Figure S4). Lack of flow compensation may cause large veins with high blood velocity to shift due to mis-encoding.[84] In this study, this problem was alleviated by manually excluding the central veins from the lesion ROI (identified and segmented by neuroradiologists experienced with brain QSM, S.Z., W.H, and I.K) from the MS lesion ROI. For capillary level vessels, flow-related issue is not expected as they exhibit very slow blood flow of less than 1 mm/sec. Spatial resolution, which scales linearly with SNR, could have an impact on OEF quantification. To investigate this issue, a numerical simulation was performed to compare OEF obtained at SNR =1000, 100, and 50 using CAT algorithm used in this study, and negligible difference in mean OEF value was found.[20] The CAT may alleviate the OEF dependency on SNR by substantially improving the effective SNR through signal averaging in clusters.[20]

Sixth, the medication effect has not been considered in the statistical analysis due to the limited sample size and variation of treatment drugs.

Seventh, though the comparison of venous oxygenation in lesion draining veins and its corresponding normal veins would be valuable to study the source of decreased OEF in the lesion core, it is difficult to perform because it is hard to specify the exact draining veins and venous oxygenation estimation may be biased due to partial volume effect. For instance, in an additional comparison, a neuroradiologist (I.K., 23 years of experience) identified central veins in 17 out of 80 lesions with thickness of 1∼2 voxels and its corresponding normal veins on contralateral side. Then, venous oxygenation in the central veins was calculated using mean QSM values[85] and compared with that in the normal veins. The venous oxygenation was similar and not significantly different between the lesion central veins and its corresponding normal veins: $88.9 \pm 1.5\%$ vs. $89.1 \pm 1.1\%$ ($\beta = -0.002$, 95% CI: [−0.012, 0.009], $p = 0.78$, linear mixed-effect model analysis). This may result from that the central veins in MS lesions are not generally the draining veins of the MS lesions.[86] Even if the draining veins are correctly identified, its oxygenation is likely to suffer from partial volume effect due to the limited resolution, e.g. 3 mm slice thickness used in this study. A higher venous oxygenation in the normal veins than previously reported venous oxygenation in large veins, 89.1% vs. 63.7%,[85] suggests that the central vein oxygenation suffers from the partial volume effect.

Finally, this study used a cross-sectional design to investigate chronic active rim lesions. We plan to perform longitudinal studies in our future work.

In conclusion, brain OEF mapping is feasible in MS brains and can detect within-lesion difference between the rim and core regions of MS lesions with QSM hyperintense rim as well as global and regional gray matter differences between MS and HC. OEF maps may provide useful information on tissue oxygenation and viability for MS monitoring and treatment.

Funding

The author(s) disclosed receipt of the following financial support for the research, authorship, and/or publication of this article: This work is supported in part by NIH K99 NS123229, R01 NS090464, R01 NS104283, R01 NS105144, S10 OD021782, and NMSS RR-1602-07671.

Declaration of conflicting interests

The author(s) declared no potential conflicts of interest with respect to the research, authorship, and/or publication of this article.

Authors' contribution

All authors (JC, TN, WH, ES, XL, IK, SZ, KG, PS, AG, SG, and YW) made substantial contribution to the concept and design, data acquisition, or data analysis and interpretation. All authors assisted in drafting or revising the article. Final approval of the submitted manuscript was provided by all authors.

ORCID iDs

Junghun Cho https://orcid.org/0000-0002-0826-5463
Shun Zhang https://orcid.org/0000-0002-0001-1880
Pascal Spincemaille https://orcid.org/0000-0002-8821-1341

Supplemental material

Supplemental material for this article is available online.

References

1. Filippi M, Bar-Or A, Piehl F, et al. Multiple sclerosis. *Nat Rev Dis Primers* 2018; 4: 49.
2. Ge Y. Multiple sclerosis: the role of MR imaging. *AJNR Am J Neuroradiol* 2006; 27: 1165–1176.
3. Polman CH, Reingold SC, Banwell B, et al. Diagnostic criteria for multiple sclerosis: 2010 revisions to the McDonald criteria. *Ann Neurol* 2011; 69: 292–302.
4. Sommer NN, Saam T, Coppenrath E, et al. Multiple sclerosis: improved detection of active cerebral lesions with 3-dimensional T1 black-blood magnetic resonance imaging compared with conventional 3-dimensional T1 GRE imaging. *Invest Radiol* 2018; 53: 13–19.
5. Vellinga MM, Oude Engberink RD, Seewann A, et al. Pluriformity of inflammation in multiple sclerosis shown

by ultra-small iron oxide particle enhancement. *Brain* 2008; 131: 800–807.
6. Lassmann H. The pathologic substrate of magnetic resonance alterations in multiple sclerosis. *Neuroimaging Clin N Am* 2008; 18: 563–576, ix.
7. Kutzelnigg A and Lassmann H. Pathology of multiple sclerosis and related inflammatory demyelinating diseases. *Handb Clin Neurol* 2014; 122: 15–58.
8. Absinta M, Sati P, Masuzzo F, et al. Association of chronic active multiple sclerosis lesions with disability in vivo. *JAMA Neurol* 2019; 76: 1474–1483.
9. Harrison DM, Li X, Liu H, et al. Lesion heterogeneity on high-field susceptibility MRI is associated with multiple sclerosis severity. *AJNR Am J Neuroradiol* 2016; 37: 1447–1453.
10. Gillen KM, Mubarak M, Park C, et al. QSM is an imaging biomarker for chronic glial activation in multiple sclerosis lesions. *Ann Clin Transl Neurol* 2021; 8: 877–812.
11. de Rochefort L, Liu T, Kressler B, et al. Quantitative susceptibility map reconstruction from MR phase data using Bayesian regularization: validation and application to brain imaging. *Magn Reson Med* 2010; 63: 194–206.
12. Kaunzner UW, Kang Y, Zhang S, et al. Quantitative susceptibility mapping identifies inflammation in a subset of chronic multiple sclerosis lesions. *Brain* 2019; 142: 133–145.
13. Yao Y, Nguyen TD, Pandya S, et al. Combining quantitative susceptibility mapping with automatic zero reference (QSM0) and myelin water fraction imaging to quantify iron-related myelin damage in chronic active MS lesions. *Ajnr Am J Neuroradiol* 2018; 39: 303–310.
14. Wang Y, Spincemaille P, Liu Z, et al. Clinical quantitative susceptibility mapping (QSM): biometal imaging and its emerging roles in patient care. *J Magn Reson Imaging* 2017; 46: 951–971.
15. Absinta M, Sati P, Gaitán MI, et al. Seven-tesla phase imaging of acute multiple sclerosis lesions: a new window into the inflammatory process. *Ann Neurol* 2013; 74: 669–678.
16. Hametner S, Wimmer I, Haider L, et al. Iron and neurodegeneration in the multiple sclerosis brain. *Ann Neurol* 2013; 74: 848–861.
17. Dal-Bianco A, Grabner G, Kronnerwetter C, et al. Slow expansion of multiple sclerosis iron rim lesions: pathology and 7 T magnetic resonance imaging. *Acta Neuropathol* 2017; 133: 25–42.
18. Eskreis-Winkler S, Zhang Y, Zhang J, et al. The clinical utility of QSM: disease diagnosis, medical management, and surgical planning. *NMR Biomed* 2017; 30: e3668.
19. Cho J, Kee Y, Spincemaille P, et al. Cerebral metabolic rate of oxygen (CMRO2) mapping by combining quantitative susceptibility mapping (QSM) and quantitative blood oxygenation level-dependent imaging (qBOLD). *Magn Reson Med* 2018; 80: 1595–1604.
20. Cho J, Zhang S, Kee Y, et al. Cluster analysis of time evolution (CAT) for quantitative susceptibility mapping (QSM) and quantitative blood oxygen level-dependent magnitude (qBOLD)-based oxygen extraction fraction (OEF) and cerebral metabolic rate of oxygen (CMRO2) mapping. *Magn Reson Med* 2020; 83: 844–857.
21. Ayton S, Faux NG and Bush AI. Association of cerebrospinal fluid ferritin level with preclinical cognitive decline in APOE-epsilon4 carriers. *JAMA Neurol* 2017; 74: 122–125.
22. Zhang J, Cho J, Zhou D, et al. Quantitative susceptibility mapping-based cerebral metabolic rate of oxygen mapping with minimum local variance. *Magn Reson Med* 2018; 79: 172–179.
23. Zhang J, Zhou D, Nguyen TD, et al. Cerebral metabolic rate of oxygen (CMRO2) mapping with hyperventilation challenge using quantitative susceptibility mapping (QSM). *Magn Reson Med* 2017; 77: 1762–1773.
24. Yablonskiy DA and Haacke EM. Theory of NMR signal behavior in magnetically inhomogeneous tissues: the static dephasing regime. *Magn Reson Med* 1994; 32: 749–763.
25. Ulrich X and Yablonskiy DA. Separation of cellular and BOLD contributions to T2* signal relaxation. *Magn Reson Med* 2016; 75: 606–615.
26. Yablonskiy DA, Sukstanskii AL and He X. BOLD-based techniques for quantifying brain hemodynamic and metabolic properties – theoretical models and experimental approaches. *NMR Biomed* 2013; 26: 963–986.
27. He X and Yablonskiy DA. Quantitative BOLD: mapping of human cerebral deoxygenated blood volume and oxygen extraction fraction: default state. *Magn Reson Med* 2007; 57: 115–126.
28. Zhang S, Cho J, Nguyen TD, et al. Initial experience of challenge-free MRI-BASED oxygen extraction fraction mapping of ischemic stroke at various stages: comparison with perfusion and diffusion mapping. *Front Neurosci* 2020; 14: 535441.
29. Cho J, Lee J, An H, et al. Cerebral oxygen extraction fraction (OEF): comparison of challenge-free gradient echo QSM+qBOLD (QQ) with 15O PET in healthy adults. *J Cereb Blood Flow Metab* 2021; 41: 1658–1668.
30. Mesaros S, Rovaris M, Pagani E, et al. A magnetic resonance imaging voxel-based morphometry study of regional gray matter atrophy in patients with benign multiple sclerosis. *Arch Neurol* 2008; 65: 1223–1230.
31. Haider L, Simeonidou C, Steinberger G, et al. Multiple sclerosis deep grey matter: the relation between demyelination, neurodegeneration, inflammation and iron. *J Neurol Neurosurg Psychiatry* 2014; 85: 1386–1395.
32. Neema M, Arora A, Healy BC, et al. Deep gray matter involvement on brain MRI scans is associated with clinical progression in multiple sclerosis. *J Neuroimaging* 2009; 19: 3–8.
33. Cifelli A, Arridge M, Jezzard P, et al. Thalamic neurodegeneration in multiple sclerosis. *Ann Neurol* 2002; 52: 650–653.
34. Ge Y, Zhang Z, Lu H, et al. Characterizing brain oxygen metabolism in patients with multiple sclerosis with T2-relaxation-under-spin-tagging MRI. *J Cereb Blood Flow Metab* 2012; 32: 403–412.
35. Fan AP, Govindarajan ST, Kinkel RP, et al. Quantitative oxygen extraction fraction from 7-tesla MRI phase:

reproducibility and application in multiple sclerosis. *J Cereb Blood Flow Metab* 2015; 35: 131–139.
36. Frischer JM, Weigand SD, Guo Y, et al. Clinical and pathological insights into the dynamic nature of the white matter multiple sclerosis plaque. *Ann Neurol* 2015; 78: 710–721.
37. Meyer-Moock S, Feng Y-S, Maeurer M, et al. Systematic literature review and validity evaluation of the expanded disability status scale (EDSS) and the multiple sclerosis functional composite (MSFC) in patients with multiple sclerosis. *BMC Neurol* 2014; 14: 58.
38. Xu B, Liu T, Spincemaille P, et al. Flow compensated quantitative susceptibility mapping for venous oxygenation imaging. *Magn Reson Med* 2014; 72: 438–445.
39. Liu T, Wisnieff C, Lou M, et al. Nonlinear formulation of the magnetic field to source relationship for robust quantitative susceptibility mapping. *Magn Reson Med* 2013; 69: 467–476.
40. Liu T, Khalidov I, de Rochefort L, et al. A novel background field removal method for MRI using projection onto dipole fields (PDF). *NMR Biomed* 2011; 24: 1129–1136.
41. Liu Z, Spincemaille P, Yao Y, et al. MEDI+0: Morphology enabled dipole inversion with automatic uniform cerebrospinal fluid zero reference for quantitative susceptibility mapping. *Magn Reson Med* 2018; 79: 2795–2803.
42. Liu J, Liu T, de Rochefort L, et al. Morphology enabled dipole inversion for quantitative susceptibility mapping using structural consistency between the magnitude image and the susceptibility map. *Neuroimage* 2012; 59: 2560–2568.
43. Wang Y and Liu T. Quantitative susceptibility mapping (QSM): decoding MRI data for a tissue magnetic biomarker. *Magn Reson Med* 2015; 73: 82–101.
44. Zhang J, Liu T, Gupta A, et al. Quantitative mapping of cerebral metabolic rate of oxygen (CMRO2) using quantitative susceptibility mapping (QSM). *Magn Reson Med* 2015; 74: 945–952.
45. Yablonskiy DA and Sukstanskii AL. Effects of biological tissue structural anisotropy and anisotropy of magnetic susceptibility on the gradient echo MRI signal phase: theoretical background. *NMR in Biomedicine* 2017; 30: e3655.
46. He X, Zhu M and Yablonskiy DA. Validation of oxygen extraction fraction measurement by qBOLD technique. *Magn Reson Med* 2008; 60: 882–888.
47. Yablonskiy DA. Quantitation of intrinsic magnetic susceptibility-related effects in a tissue matrix. Phantom study. *Magn Reson Med* 1998; 39: 417–428.
48. Cho J, Spincemaille P, Nguyen TD, et al. Combined cluster analysis of time evolution and tissue type with total variation denoising (CCTV) for QQ-based oxygen extraction fraction mapping. In: *Proceedings of the 29th international society of magnetic resonance in medicine annual meeting*, Virtual, 15–20 May 2021, p.1283. Berkeley, CA: International Society for Magnetic Resonance in Medicine.
49. Cho J, Spincemaille P, Nguyen TD, et al. Temporal clustering, tissue composition, and total variation for mapping oxygen extraction fraction using QSM and quantitative BOLD. *Magn Reson Med*. Epub ahead of print 10 June 2021. DOI: 10.1002/mrm.28875.
50. Zhang Y, Brady M and Smith S. Segmentation of brain MR images through a hidden Markov random field model and the expectation-maximization algorithm. *IEEE Trans Med Imaging* 2001; 20: 45–57.
51. Rudin LI, Osher S and Fatemi E. Nonlinear total variation based noise removal algorithms. *Physica D: Nonlinear Phenomena* 1992; 60: 259–268.
52. Li J, Chang S, Liu T, et al. Reducing the object orientation dependence of susceptibility effects in gradient echo MRI through quantitative susceptibility mapping. *Magn Reson Med* 2012; 68: 1563–1569.
53. Fischl B, Salat DH, Busa E, et al. Whole brain segmentation: automated labeling of neuroanatomical structures in the human brain. *Neuron* 2002; 33: 341–355.
54. Houtchens MK, Benedict RHB, Killiany R, et al. Thalamic atrophy and cognition in multiple sclerosis. *Neurology* 2007; 69: 1213–1223.
55. Benjamini Y and Hochberg Y. Controlling the false discovery rate: a practical and powerful approach to multiple testing. *J R Stat Soc Series B (Methodological)* 1995; 57: 289–300.
56. Jarque CM and Bera AK. A test for normality of observations and regression residuals. *Int Stat Rev/Revue Internationale de Statistique* 1987; 55: 163–172.
57. Wisnieff C, Ramanan S, Olesik J, et al. Quantitative susceptibility mapping (QSM) of white matter multiple sclerosis lesions: interpreting positive susceptibility and the presence of iron. *Magn Reson Med* 2015; 74: 564–570.
58. Mintun MA, Raichle ME, Martin WR, et al. Brain oxygen utilization measured with O-15 radiotracers and positron emission tomography. *J Nuclear Med* 1984; 25: 177–187.
59. Raichle ME, MacLeod AM, Snyder AZ, et al. A default mode of brain function. *Proc Natl Acad Sci USA* 2001; 98: 676–682.
60. Yang R and Dunn JF. Reduced cortical microvascular oxygenation in multiple sclerosis: a blinded, case-controlled study using a novel quantitative near-infrared spectroscopy method. *Sci Rep* 2015; 5: 16477.
61. Sun X, Tanaka M, Kondo S, et al. Clinical significance of reduced cerebral metabolism in multiple sclerosis: a combined PET and MRI study. *Ann Nucl Med* 1998; 12: 89–94.
62. Brown GC and Borutaite V. Nitric oxide inhibition of mitochondrial respiration and its role in cell death. *Free Radic Biol Med* 2002; 33: 1440–1450.
63. Encinas JM, Manganas L and Enikolopov G. Nitric oxide and multiple sclerosis. *Curr Neurol Neurosci Rep* 2005; 5: 232–238.
64. Smith KJ and Lassmann H. The role of nitric oxide in multiple sclerosis. *Lancet Neurol* 2002; 1: 232–241.

65. Su KG, Banker G, Bourdette D, et al. Axonal degeneration in multiple sclerosis: the mitochondrial hypothesis. *Curr Neurol Neurosci Rep* 2009; 9: 411–417.
66. Varghese J, Potter LC, LaFountain R, et al. CMR-based blood oximetry via multi-parametric estimation using multiple T2 measurements. *J Cardiovasc Magn Reson* 2017; 19: 88.
67. Hagemeier J, Zivadinov R, Dwyer MG, et al. Changes of deep gray matter magnetic susceptibility over 2 years in multiple sclerosis and healthy control brain. *Neuroimage Clin* 2018; 18: 1007–1016.
68. Alexander GE and Crutcher MD. Functional architecture of basal ganglia circuits: neural substrates of parallel processing. *Trends Neurosci* 1990; 13: 266–271.
69. Bergsland N, Zivadinov R, Dwyer MG, et al. Localized atrophy of the thalamus and slowed cognitive processing speed in MS patients. *Mult Scler* 2016; 22: 1327–1336.
70. Rocca MA, Mesaros S, Pagani E, et al. Thalamic damage and long-term progression of disability in multiple sclerosis. *Radiology* 2010; 257: 463–469.
71. Stuber C, Pitt D and Wang Y. Iron in multiple sclerosis and its noninvasive imaging with quantitative susceptibility mapping. *Int J Mol Sci* 2016; 17: 100.
72. Kirui DK, Khalidov I, Wang Y, et al. Targeted near-IR hybrid magnetic nanoparticles for in vivo cancer therapy and imaging. *Nanomedicine* 2013; 9: 702–711.
73. Persson N, Wu J, Zhang Q, et al. Age and sex related differences in subcortical brain iron concentrations among healthy adults. *NeuroImage* 2015; 122: 385–398.
74. Langkammer C, Liu T, Khalil M, et al. Quantitative susceptibility mapping in multiple sclerosis. *Radiology* 2013; 267: 551–559.
75. Schweser F, Hagemeier J, Dwyer MG, et al. Decreasing brain iron in multiple sclerosis: the difference between concentration and content in iron MRI. *Hum Brain Mapp* 2021; 42: 1463–1474.
76. Langkammer C, Krebs N, Goessler W, et al. Susceptibility induced gray-white matter MRI contrast in the human brain. *Neuroimage* 2012; 59: 1413–1419.
77. Chen W, Gauthier SA, Gupta A, et al. Quantitative susceptibility mapping of multiple sclerosis lesions at various ages. *Radiology* 2014; 271: 183–192.
78. Murphy WG. The sex difference in haemoglobin levels in adults – mechanisms, causes, and consequences. *Blood Rev* 2014; 28: 41–47.
79. Ibaraki M, Shinohara Y, Nakamura K, et al. Interindividual variations of cerebral blood flow, oxygen delivery, and metabolism in relation to hemoglobin concentration measured by positron emission tomography in humans. *J Cereb Blood Flow Metab* 2010; 30: 1296–1305.
80. Qin Q, Grgac K and van Zijl PC. Determination of whole-brain oxygen extraction fractions by fast measurement of blood T(2) in the jugular vein. *Magn Reson Med* 2011; 65: 471–479.
81. Zivadinov R, Galeotti R, Hojnacki D, et al. Value of MR venography for detection of internal jugular vein anomalies in multiple sclerosis: a pilot longitudinal study. *Ajnr Am J Neuroradiol* 2011; 32: 938–946.
82. Wattjes MP, van Oosten BW, de Graaf WL, et al. No association of abnormal cranial venous drainage with multiple sclerosis: a magnetic resonance venography and flow-quantification study. *J Neurol Neurosurg Psychiatry* 2011; 82: 429–435.
83. D'Haeseleer M, Cambron M, Vanopdenbosch L, et al. Vascular aspects of multiple sclerosis. *Lancet Neurol* 2011; 10: 657–666.
84. Larson TC, Kelly WM, Ehman RL, et al. Spatial misregistration of vascular flow during MR imaging of the CNS: cause and clinical significance. *AJR Am J Roentgenol* 1990; 155: 1117–1124.
85. Fan AP, Bilgic B, Gagnon L, et al. Quantitative oxygenation venography from MRI phase. *Magn Reson Med* 2014; 72: 149–159.
86. Adams CWM. The onset and progression of the lesion in multiple sclerosis. *J Neurol Sci* 1975; 25: 165–182.